Annealing of RF-magnetron sputtered SnS_2 precursors as a new route for single phase SnS thin films

M.G. Sousa, A.F. da Cunha, P.A. Fernandes

ABSTRACT

Tin sulphide thin films have been grown on soda-lime glass substrates through the annealing of RF-magnetron sputtered SnS_2 precursors. Three different approaches to the annealing were compared and the resulting films thoroughly studied. One series of precursors was annealed in a tubular furnace directly exposed to a flux of sulphur vapour plus forming gas, $N_2 + 5\%H_2$, and at a constant pressure of 500 mbar. The other two series of identical precursors were annealed in the same furnace but inside a graphite box with and without elemental sulphur evaporation again in the presence of $N_2 + 5\%H_2$ and at the same pressure as for the sulphur flux experiments. Different maximum annealing temperatures for each set of samples, in the range of 300–570 °C, were tested to study their effects on the properties of the final films. The resulting phases were structurally investigated by X-Ray Diffraction (XRD) and Raman spectroscopy. Annealing of SnS_2 precursors in sulphur flux produced films where SnS_2 was dominant for temperatures up to 480 °C. Increasing the temperature to 530 °C and 570 °C led to films where the dominant phase became Sn_2S_3. Annealing of SnS_2 precursors in a graphite box with sulphur vapour at temperatures in the range between 300 °C and 480 °C the films are multi-phase, containing Sn_2S_3, SnS_2 and SnS. For high annealing temperatures of 530 °C and 570 °C the films have SnS as the dominant phase. Annealing of SnS_2 precursors in a graphite box without sulphur vapour at 300 °C and 360 °C the films are essentially amorphous, at 420 °C SnS_2 is the dominant phase. For temperatures of 480 °C and 530 °C SnS is the dominant phase but also same residual SnS_2 and Sn_2S_3 phases are observed. For annealing at 570 °C, according to the XRD results the films appear to be single phase SnS. The composition was studied using energy dispersive spectroscopy being then correlated with the annealing temperature. Scanning electron microscopy studies revealed that the SnS films exhibit small grain structure and the film surface is rough. Optical measurements were performed, from which the band gap energies were estimated. These studies show that the direct absorption transitions of SnS are at 1.68 eV and 1.41 eV for annealing in graphite box with and without elemental sulphur evaporation, respectively. For the indirect transition the values varied from 1.49 eV to 1.37 eV. The results of this work show that the third approach is better suited to produce single phase SnS films. However, a finer tunning of the duration of the high temperature plateau of the annealing profile is required in order to eliminate the β-Sn top layer.

1. Introduction

The replacement of CuIn$_{1-x}$Ga$_x$Se$_2$ as solar cell absorber by In-free compounds has motivated the research on new materials such as tin sulphide, SnS. Theoretical studies point out its potential for photovoltaic applications [1–3]. There are many advantages of SnS such as suitable band gap (∼1.3 eV), large absorption coefficient ($> 10^4$), low cost, non-toxic and based on abundant elements [4,5]. Despite these advantages, single phase films appear to be difficult to grow due to the formation of other phases during the annealing process such as, SnS$_2$ and Sn$_2$S$_3$. As SnS has a high vapour pressure, losses of material occur at high processing temperatures. Therefore, this difficulty is increased when growth is performed in a vacuum system. In the literature, thin films of SnS have been prepared by several methods including thermal evaporation [6–9], electron beam evaporation [10,11], spray pyrolysis [12], electrodeposition [13,14], chemical bath deposition (CBD) [15–19], sol–gel [20] vacuum evaporation [21] and dc magnetron sputtering [22]. Each method has its own characteristics in producing homogeneous and defect free thin film materials. The attempts to use SnS in device structures are limited but previous studies have reported solar cells with efficiencies up to ∼2.04% [23]. The aim of this work is to try to find a route to produce single phase SnS thin films from SnS$_2$ precursors. Three different approaches based on the annealing of RF-magnetron sputtered SnS$_2$ precursors have been followed. We report here, a systematic and detailed study of the effects of the annealing conditions on the phase content of the tin sulphide films.

2. Experimental methods

In this work, the method used for the growth of tin sulphide thin films consisted on the annealing of RF-magnetron sputtered SnS$_2$ precursors.Three sets of samples have been prepared. The SnS$_2$ precursor layers with purity of ∼99.99% were deposited by RF-magnetron sputtering on soda lime glass (SLG) substrates cleaned in sucessive ultrasound baths of acetone/ethanol/deionised water and finally dried with a N$_2$ flow. The base pressure of the sputtering system was 10^{-5} mbar. The deposition was done in an Ar + 10%H$_2$ atmosphere, at an operating pressure of 4.0×10^{-3} mbar. After the deposition of the precursor layer, the samples were transfered to a tubular furnace where annealing was performed at a constant working pressure of 500 mbar either in a flux of sulphur vapour plus forming gas, N$_2$ + 5%H$_2$, at flow rate of 40 ml min^{-1} or in a closed graphite box with and without elemental sulphur evaporation. In the first series of samples, sulphur is evaporated by a source located at the left end of the furnace at a temperature of 230 °C. The sulphur vapour is transported, with the help of a N$_2$ + 5%H$_2$ flux, along the furnace. For the second series of samples, 100 mg of high purity sulphur shots (∼99.999%) were evaporated inside a graphite box while in the third series, no sulphur vapour is present. For each series, the annealing temperature profiles had a maximum plateau which varied from 300 °C to 570 °C and lasted 15 min. The thicknesses of the final annealed layers were measured using a Dektak 150 step profiler. The morphology and average composition were analysed by SEM, Hitachi Su-70 equipped with a Rontec EDS system. The crystalline structure was analysed by X-Ray Diffraction (XRD) with a Philips PW 3710 system, in the Bragg–Brentano configuration (θ–2θ), using the Cu Kα line (wavelength λ = 1.54060 Å) and the generator settings were 50 mA and 40 KV. A LabRam Horiba, HR800 UV spectrometer, equipped with a solid state laser oscillating at 532 nm was used for the Raman scattering measurements. Optical measurements were done using a Shimadzu UV3600 spectrophotometer equipped with an integrating sphere. The sample naming scheme makes reference to the annealing conditions and maximum temperature.The S in the first series means that the annealing was performed in a flux of sulphur vapour. SGBS and SGB means that the annealing was performed in a graphite box with and without elemental sulphur evaporation, respectively. All the acronyms are followed by the maximum annealing temperature. For a summary see Table 1.

Table 1
Sample labelling and summary of the different annealing approaches.

Sample name	Sulphur	Graphite box	Annealing temperature (°C)
S300 → S570	Flux	No	300–570
SGBS300 → SGBS570	Pieces	Yes	300–570
SGB300 → SGB570	–	Yes	300–570

3. Results and discussion

The work reported in this study aims at establishing a suitable route to prepare single phase SnS thin films. Three series of samples were prepared following three different annealing approaches. For each case, the annealing temperatures were 300 °C, 360 °C, 420 °C, 480 °C, 530 °C and 570 °C. In order to simplify the presentation of the results data are only presented for the selected temperatures of 300 °C, 480 °C and 570 °C, except for XRD.

Table 2 shows the results of the compositional analysis as well as the thicknesses for the studied samples. For the first series, no clear trend for the Sn:S ratio is observed. For samples S300 and S570 the ratio is around 0.65 which is compatible with Sn$_2$S$_3$ being the dominant phase. For S480 the Sn:S ratio was 0.55 which points to SnS$_2$ as the dominant phase. For the second and third series, the Sn:S ratio increased with increasing annealing temperature. Nevertheless, there are differences between these two series. In the second series of samples (SGBS300 to SGBS570) the composition ratios increased from 0.6 at 300 °C to near stoichiometric at 570 °C. In the case of the third series while sample SGB300 has Sn:S ratio below 1 samples SGB480 and SGB570 present a ratio higher than 1. These latter results suggest that the samples are tin rich.

The SEM images of the samples are shown in Fig. 1. This analysis revealed that the samples annealed at lower temperatures exhibited small grain structure uniformly distributed and good coverage of the substrate surface. A dense structure can be observed. The sample S570 is not as dense as the sample prepared at 300 °C but is composed of extended grains. Voids and cracks were found in the samples S570, SGB570 and SGBS570. As the maximum annealing temperature increased from 300 °C to 480 °C, the surface roughness increased for the three sets of samples. However, when the temperature was increased further, from 480 °C to 570 °C, the surface roughness decreased.

Fig. 2 shows the XRD diffractograms for samples S300 to S570 (a), SGBS300 to SGBS570 (b) and SGB300 to SGB570 (c). In the first series of samples, Fig. 2a, and according to the International Centre for Diffraction Data (ICDD), for the lowest temperature (300 °C), the sample consists on a mixture of orthorhombic Sn$_2$S$_3$ and hexagonal SnS$_2$ phases. Increasing the temperature to 360 °C and then to 420 °C, the amount of Sn$_2$S$_3$ (Reference code: 04-008-2097) present decreased substantially and SnS$_2$ become the dominant phase. Well defined peaks at 2θ = 15.02°, 30.19°, 46.01° and 62.82° match the standard pattern for the mineral Berndtite-2T (Reference code: 00-023-0677) with SnS$_2$ composition and correspond to the crystallographic planes: (001), (002), (003) and (004), respectively. For 480 °C again phases corresponding to Sn$_2$S$_3$ appear. Increasing further the temperature to 530 °C and 570 °C, there is a decrease in the intensity of the peaks related to the SnS$_2$ phase and the dominant

Table 2
Composition ratios and thickness for the three series of samples prepared with three different annealing approaches of RF-magnetron sputtered SnS$_2$ precursors and grown on soda lime glass substrates.

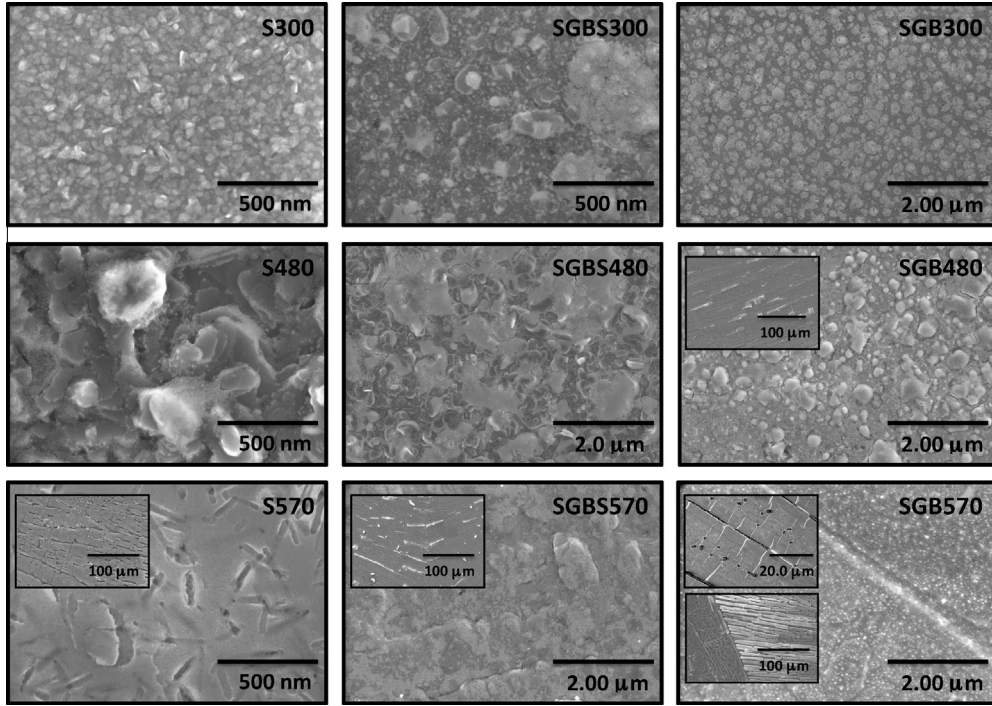| Thickness (nm) SnS$_2$ precursor	Sample	Sn (at.%)	S (at.%)	$\frac{Sn}{S}$
∼320	S300	18.45	28.34	0.65
	S480	9.23	16.75	0.55
	S570	5.39	8.40	0.64
	SGBS300	4.24	6.36	0.58
	SGBS480	5.23	7.24	0.72
	SGBS570	3.62	3.92	0.92
	SGB300	4.93	6.91	0.71
	SGB480	2.89	2.29	1.26
	SGB570	3.75	2.38	1.57

Fig. 1. SEM micrographs for the samples annealed in a flux of sulphur vapour (left column) and in a graphite box with (middle column) and without (right column) elemental sulphur evaporation. The morphology was analysed by SEM, Hitachi Su-70 equipped with a Rontec EDS system operated at an acceleration voltage of 4.0 KV. The inset of images within several figures shows the morphology using the same system but with an acceleration voltage of 25 KV.
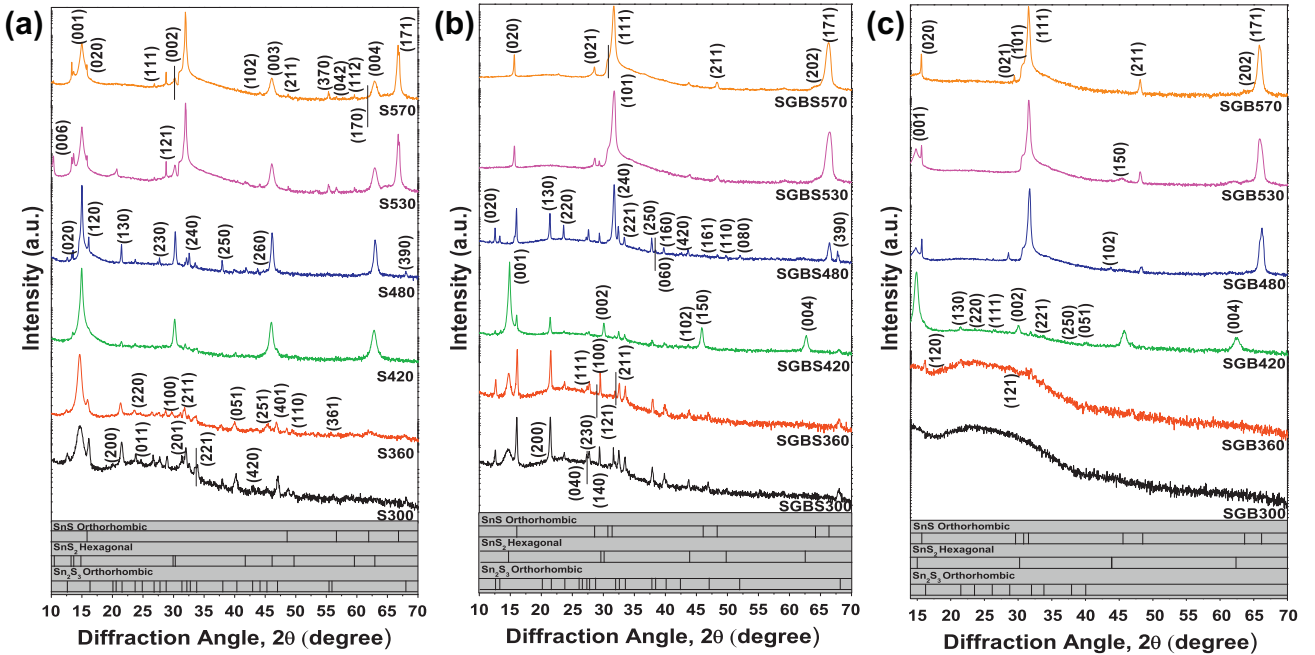

Fig. 2. XRD diffractograms for the samples annealed in a flux of sulphur vapour (a) and in a graphite box with (b) and without (c) elemental sulphur evaporation.

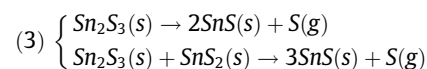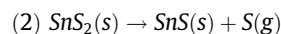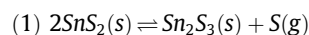phase becomes Sn_2S_3. Orthorhombic SnS phases were also detected in these samples.

In the second series of samples, Fig. 2b, for 300 °C and 360 °C, it is observed that the samples are multi-phase, containing Sn_2S_3, SnS_2 and SnS. Increasing the temperature to 420 °C, the Sn_2S_3 phase decreases substantially and promotes the formation of SnS_2 as dominant phase. At 480 °C, started to emerge as the dominant phase but Sn_2S_3 is still present. The peaks corresponding to SnS_2, observed at lower temperature, now disappeared. When

the temperature was increased to 570 °C, the corresponding XRD pattern suggests that the films are mostly SnS however traces SnS_2 and Sn_2S_3 are still present. The EDS measurements of these samples (Table 1) indicated that the ratio of Sn:S had increased and that for the higher annealing temperatures the samples tended towards a stoichiometric ratio of 1:1.

In the third series of samples, Fig. 2c, for 300 °C and 360 °C, the XRD pattern of the samples shows no obvious diffraction peaks, indicating that the samples are amorphous. For 420 °C the domi-

nant phase matches SnS_2 but Sn_2S_3 and SnS phases are also present. At 480 °C, there is a decrease in the intensity of the peaks related to SnS_2 and an increase in the SnS phase. The latter becomes dominant, however, SnS_2 and Sn_2S_3 phases are still present to some extent. Increasing further the temperature to 530 °C, promotes the formation of SnS. The XRD pattern also shows a small additional peak which comes from trace amounts of SnS_2. For 570 °C, the film is single phase SnS according to XRD. Three major diffraction peaks appear at $2\theta = 15.72°$, 31.51° and 65.76° which are assigned to (020), (111) and (222) reflections of orthorhombic SnS. The EDS analysis revealed that these films were tin rich. These changes in the XRD patterns, lead to the conclusion that as the temperature increases to 570 °C, loss of sulphur exists leading to the preferential formation of SnS in detriment of other phases with higher sulphur content.

The structural analysis' results show that the formation of different Sn_xS_y phases with the change of the maximum temperature and the annealing approach may be interpreted as the result of different dissociation reactions, as given below:

(1) $2SnS_2(s) \rightleftharpoons Sn_2S_3(s) + S(g)$

(2) $SnS_2(s) \rightarrow SnS(s) + S(g)$

(3) $\begin{cases} Sn_2S_3(s) \rightarrow 2SnS(s) + S(g) \\ Sn_2S_3(s) + SnS_2(s) \rightarrow 3SnS(s) + S(g) \end{cases}$

Considering the samples annealed in a flux of sulphur vapour (S300 to S570), for lower temperatures a mixture of SnS_2 and Sn_2S_3 phases were observed. The formation of Sn_2S_3 from SnS_2 precursors and S vapour may be interpreted as the result of the dissociation reaction defined as (1). Increasing further the temperature, the reverse process of this reaction appears to occur, promoting the formation of SnS_2 as dominant phase, at a temperature of 420 °C. At 530 °C and 570 °C, a clear evidence of decomposition of SnS_2 into Sn_2S_3 occurs again, becoming the latter dominant. For graphite box experiments (SGBS300 to SGBS570 and SGB300 to SGB570) the results indicate that for annealing temperatures ranging from 300 °C to 480 °C the samples are multi-phase, containing Sn_2S_3, SnS_2 and SnS. In addition to the reaction (1), it is possible that some SnS_2 phases present are converted into SnS, according to reaction (2). At high temperatures (570 °C), the XRD pattern suggests that the film SGB570 is single phase. The formation of this phase can occur through the reactions (3) and may be attributed to conversion of Sn_2S_3 and SnS_2 phases into SnS.

Fig. 3 shows the Raman scattering spectra for the samples annealed at the highest temperature for each annealing approach (S570, SGBS570 and SBG570). Raman analysis of the sample S570 confirmed the presence of SnS_2 with a peak at 314.5 cm^{-1} [22,24]. Other phases with vibrational modes located at 162.3 cm^{-1}, 191.9 cm^{-1}, 220.1 cm^{-1} and 267.8 cm^{-1} were also detected and assigned to the SnS phase [24–26]. A weak intensity mode located at 256.3 cm^{-1} was also detected corresponding to the Sn_2S_3 phase [24]. A clear difference in the information extracted from the XRD and Raman spectrum is that while the analysis of XRD pattern suggested that Sn_2S_3 is dominant, the Raman results point to SnS_2 as the dominant phase. The Raman spectrum shows a strong peak characteristic of SnS_2 at 314.5 cm^{-1} but no clear evidence for Sn_2S_3. This difference between XRD and the Raman results may be do to the fact that the SnS_2 Raman signal originates close to the top surface while the XRD signal is an average from all the film thickness.

The Raman spectrum of the sample SGBS570 shows peaks at 84.9 cm^{-1}, 162.1 cm^{-1}, 175.2 cm^{-1}, 191.7 cm^{-1} and 220.1 cm^{-1} which are assigned to the SnS phase [24,27]. A weak peak located at 58.2 cm^{-1} is also observed and attributed to the Sn_2S_3 phase
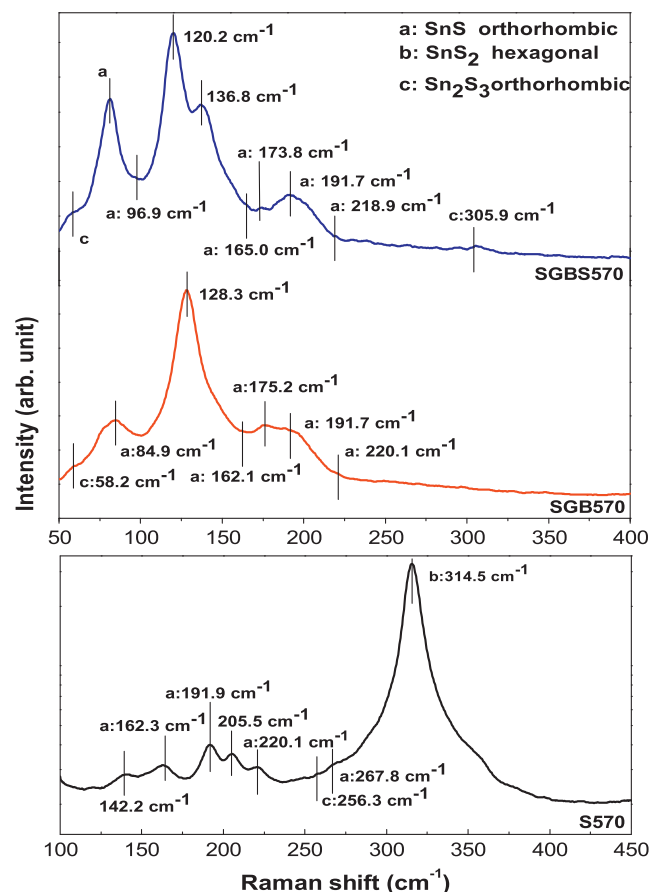

Fig. 3. Raman scattering spectra of the samples annealed at a maximum temperature of 570 °C for each annealing approach studied. Annealing in a flux of sulphur vapour (S570) and in a graphite box with (SGBS570) and without (SGB570) elemental sulphur evaporation. Raman scattering excitation was produced with a solid state laser at the wavelength of 532 nm.

[24,28]. The sample SGB570 has vibrational modes similar to the SGBS570 but in this case the intensity of the mode assigned to SnS at 84.9 cm^{-1} increased substantially. This is in agreement with the observation made in XRD since it pointed to a single phase SnS film. For SGBS570, a strong peak is observed at 128.3 cm^{-1} which does not correspond to the known Raman modes of SnS. Pressure dependent Raman scattering studies on β-Sn, reported in the literature, showed LO and TO modes at 42.4 cm^{-1} and 126.6 cm^{-1}, respectively. At atmospheric pressure the TO mode is predominant [27]. Based on this, the mode located at 128.3 cm^{-1} in our study can be assigned to the TO mode of β-Sn. Since in XRD no β-Sn was detected, for this sample, it means that it corresponds to a very thin layer at the top surface. For SGB570 the peak located at 128.3 cm^{-1}, in the case of SGBS570, unfolds into two broad bands located at 120.2 cm^{-1} and 136.8 cm^{-1}. The existence of this top β-Sn layer is, in this case, further supported by the compositional analysis which shows a Sn:S ratio greater than 1 as can be confirmed in Table 1. Fig. 3 shows that the mode assigned to the β-Sn phase is present in the samples sulphurized in the graphite box but not in the samples sulphurized with sulphur flux. This is expected since, in the latter case, a continuous supply of sulphur occurs while in the case of the graphite box, as the sulphurization proceeds, it is likely that the atmosphere becomes sulphur depleted leading to the surface SnS decomposition.

In Fig. 4, the results of the absorption edge estimation are presented for the samples annealed at the highest temperature
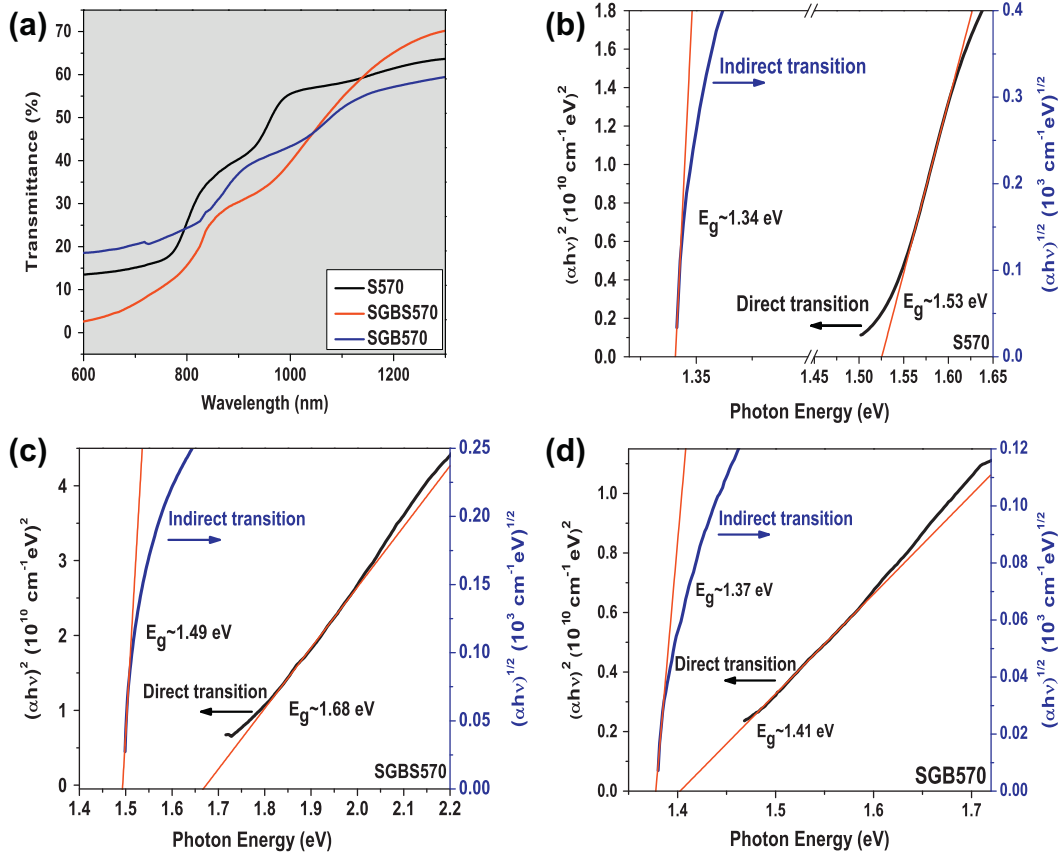
Fig. 4. Absorption edge analysis for the samples annealed at maximum temperatures of 570 °C for each annealing approach studied. Annealing in a flux of sulphur vapour (S570) and in a graphite box with (SGBS570) and without (SGBS570) elemental sulphur evaporation.

(570 °C) for each annealing approach. Fig. 4a shows the transmittance versus wavelength behaviour for S570, SGBS570 and SGB570. Fig. 4b–d shows the absorption edges estimation method and the corresponding values for direct and indirect transitions. The results in Fig. 4b, for sample S570, show an indirect transition energy of 1.34 eV and an direct transition energy of 1.53 eV. It follows from the discussion above that this sample is a solid mixture of Sn_2S_3, SnS_2 and SnS, therefore we cannot assigned these transition energies to any of the phases. For samples SGBS570 and SGB570, Fig. 4c and d shows indirect transitions at 1.49 eV and 1.37 eV, respectively. These values are considerably higher than 1.07 eV predicted for the indirect transition of SnS [1] eventhough the structural analysis, presented above, suggests that SnS is the dominant phase in these samples. This discrepancy may be the result of the existence of a very thin layer of β-Sn on the top of those samples since it will affect the reflectance and transmittance measurements and hence the absorption data. Another contribution to explain the discrepancy may be found in [9] where it is shown that the indirect transition energy of SnS films with a thickness of 750 nm has a value of 1.32 eV which is closed to the value we found for sample SGB570. That same reference also shows that the transition energy increases with decreasing film thickness. For sample SGB570 we found a direct transition energy of 1.41 eV which is in the range theoretically predicted [1]. This is in agreement with the conclusions drawn from the structural analysis which pointed to SnS as the dominant phase but capped by a very thin β-Sn layer. For direct transitions we do not expect that the thin β-Sn layer affects the estimation of the corresponding energies as much as for indirect transitions since absorption of photons with energy above the transition threshold is very strong and therefore dominates over the effect of the Sn layer.

4. Conclusions

This work describes three different attempts to produce single phase SnS thin films with orthorhombic structure, consisting on the annealing of RF-magnetron sputtered SnS_2 precursors. In the first attempt these samples were annealed in a constant sulphur flux and it was observed that a solid mixture of the SnS, SnS_2 and Sn_2S_3 phases occured for all annealing temperatures. In the second attempt annealing was performed in a closed graphite box during which pieces of sulphur were evaporated. It was observed that at highest annealing temperature of 570 °C the films were predominantly formed by the SnS phase but residual amounts of Sn_2S_3 were also detected as well as a thin top layer of β-Sn. In the third attempt the SnS_2 were annealed in a closed graphite box without sulphur evaporation. The bulk of the resulting films appear to be single phase SnS and it is again capped by a thin layer of β-Sn. The results of this work show that the third approach is better suited to produce single phase SnS films. However, a finer tunning of the duration of the high temperature plateau of the annealing profile is required in order to eliminate the β-Sn top layer.

References

[1] J. Vidal, S. Lany, M. d'Avezac, A. Zunger, A. Zakutayev, J. Francis, J. Tate, Appl. Phys. Lett. 100 (2012) 032104.

[2] V. Robles, J.F. Trigo, C. Guilln, J. Herrero, J. Mater. Sci. 48 (2013) 3943–3949.
[3] K. Hartman, J.L. Johnson, M.I. Bertoni, D. Recht, M.J. Aziz, M.A. Scarpulla, T. Buonassisi, Thin Solid Films 519 (2011) 7421–7424.
[4] P. Sinsermsuksakul, J. Heo, W. Noh, A.S. Hock, R.G. Gordon, Adv. Eng. Mater. 1 (2011) 1116–1125.
[5] B. Ghosh, M. Das, P. Banerjee, S. Das, Appl. Surf. Sci. 254 (2008) 6436–6440.
[6] R.W. Miles, O.E. Ogah, G. Zoppi, I. Forbes, Thin Solid Films 517 (2009) 4702–4705.
[7] S. Cheng, G. Conibeer, Thin Solid Films 520 (2011) 837–841.
[8] P.A. Nwofe, K.T.R. Reddy, G. Sreedevi, J.K. Tan, I. Forbes, R.W. Miles, Energy Proc. 15 (2012) 354–360.
[9] A.E. Abdelrahman, W.M.M. Yunus, A.K. Arof, J. Non-Cryst. Solids 358 (2012) 1447–1451.
[10] O.E. Ogah, G. Zoppi, I. Forbes, R.W. Miles, Thin Solid Films 517 (2009) 2485.
[11] A. Tanusevski, D. Poelman, Sol. Energy Mater. Sol. Cells 80 (2003) 297.
[12] M.C. Rodriguez, H. Martinez, A.S. Juarez, J.C. Alvarez, A.T. Silver, M.E. Calixto, Thin Solid Films 517 (2009) 2497–2499.
[13] S. Cheng, Y. He, G. Chen, Mater. Chem. Phys. 110 (2008) 449–453.
[14] G. Hue, D.L. Peng, P.X. Yan, L.S. Wang, W. Wang, X.H. Luo, J. Alloys Comp. 468 (2009) 254–257.
[15] P.P. Hankare, A.V. Jadhav, P.A. Chate, K.C. RAthod, P.A. Chavan, S.A. Ingloe, J. Alloys Comp. 463 (2008) 581–584 (CBD).
[16] A. Akkari, C. Guasch, N. Kamoun-Turki, J. Alloys Comp. 490 (2010) 180–183 (CBD).
[17] C. Gao, H. Shen, Thin Solid Films 520 (2012) 3523–3527.
[18] Y. Jayasree, U. Chalapathi, P.U. Bhaskar, V.S. Raja, Appl. Surf. Sci. 258 (2012) 2732–2740.
[19] C. Gao, H. Shen, L. Sun, Z. Shen, Mater. Lett. 65 (2011) 1413–1415.
[20] C.C. Huang, Y.J. Lin, C.Y. Chuang, C.J. Liu, Y.W. Yang, J. Alloys Comp. 553 (2013) 208–211.
[21] R.W. Miles, O.E. Ogah, G. Zoppi, I. Forbes, Thin Solid Films 517 (2009) 4702–4705.
[22] J. Malaquias, P.A. Fernandes, P.M.P. Salomé, A.F. da Cunha, Thin Solid Films 519 (2011) 7416–7420.
[23] P. Sinsermsuksakul, K. Hartman, S.B. Kim, J. Heo, L. Sun, H.H. Park, R. Chakraborty, T. Buonassisi, R.G. Gordon, Appl. Phys. Lett. 102 (2013) 053901.
[24] N.R. Mathews, C.C. Garca, I.Z. Torres, Mater. Sci. Semicond. Process. 16 (2013) 29–37.
[25] L.L. Cheng, M.H. Liu, M.X. Wang, S.C. Wang, G.D. Wang, Q.Y. Zhou, Z.Q. Chen, J. Alloys Comp. 545 (2012) 122–129.
[26] G.H. Yue, Y.D. Lin, X. Wen, L.S. Wang, Y.Z. Chen, Appl. Phys. A 106 (2012) 87–91.
[27] S. Sohila, M. Rajalakshmi, C. Ghosh, A.K. Arora, C. Muthamizhchelvan, J. Alloys Comp. 509 (2011) 5843–5847.
[28] E. Guneri, F. Gode, B. Boyarbay, C. Gumus, Mater. Res. Bull. 47 (2012) 3738–3742.